UNIVERSITY OF PARDUBICE
FACULTY OF CHEMICAL TECHNOLOGY

DOCTOR THESIS

2018 **Ing. Jaroslav Kocík**

UNIVERSITY OF PARDUBICE
FACULTY OF CHEMICAL TECHNOLOGY
DEPARTMENT OF PHYSICAL CHEMISTRY

Using of mixed oxides in transesterification and aldol condensation

Author: Ing. Jaroslav Kocík

Superviser: Doc. Ing. Martin Hájek, Ph.D.

2018

Content

Abstract

The thesis is focused on the study of properties of Mg-Al, Mg-Fe, Zn-Al and Ca-Al mixed oxides, which were prepared by thermal pre-treatment of hydrotalcites in different temperatures. The hydrotalcites were prepared by co-precipitation method. The layered structure of hydrotalcites was studied by X-ray diffraction analysis and the thermal decomposition of hydrotalcite was studied by TGA-MS. The main aims of the thesis are the description of the structure properties (crystal size), the texture properties (specific surface area) and the acid-basic properties (total amount of acid and base sites) of hydrotalcites and mixed oxides with different bi- and trivalent cations. The thesis is also focused on the description of dependence of molar ratio Mg/Al and Mg/Fe on the crystal composition and texture and acid-basic properties of mixed oxides. These properties were compared with catalytic properties in aldol-condensation of furfural with acetone and transesterification rapeseed oil with methanol. My thesis is focused also on the description of properties of Mg-Al, Mg-Fe, Zn-Al and Ca-Al hydrotalcites and mixed oxides with molar ration of M^{2+}/M^{3+} = 2. The differences of these materials were presented and their properties were compared with catalytic properties in aldol condensation. The study was also focused on description of the stability of Ca-Al mixed oxides in transesterification of rapeseed oil with methanol.

1 Introduction

Developing of human society and raising its standard of living is associated with an increase in energy consumption. Worldwide energy consumption has grown steadily since the industrial revolution in the 18th century. Despite the high investment in energy-saving devices (LED bulbs, smart grids, home insulation, etc.), there is still an increase in energy consumption (about 5 % per year [1]). The United States of America and the China are among the world's largest energy consumers. There are a lot of energy sources around the world, but most of them are limited - non-renewable (coal, oil, natural gas, uranium). The climate change, the peak of non-renewable energy production, political and socio-economic factors have led to the study of alternative energy sources, which are also referred to as renewable. European Union determined that the percentage of biofuel (fuel from renewable sources) in fuels will be 10 % in 2020. Therefore the new ways for production of biofuel are intensively studied. [2].

2 Biofuels

Biofuels are one of the kind of renewable sources of energy, which can be prepared by thermochemical, chemical or biochemical methods as sugar fermentation, pyrolysis or gasification of biomass [1, 2]. Biodiesel, bioethanol or other types of biofuels can be used combustion engines. The biofuels can be divided on biofuels of first, second and third generation [3, 4]. The biofuels are divided by sources which are used for their production. The biofuels of the first generation are prepared from the sources, which can be used in food industry such as vegetable oil, animal fats, sugar cane, sugar beet etc. [5]. Biodiesel and bioethanol are the biofuels of first generation.

On the other hand, the biofuels of second generation are prepared from sources, which cannot be used in food industry, from no edible sources such as no edible oil (Jatropha, tall oil) or waste cooking oil or biomass. The physico-chemical properties are more similar to convention fuel (prepared from crude oil) than biofuel of first generation, which are prepared from crude oil [6].

The biofuels of third generation are prepared from algae. Algae are grown in fotobioreactors, which could be open (ponds) or closed as sheets, annular or tubular

fotobioreactors. The benefits of used algae for biofuel production is, that the growing of algae not consumption of the agricultural soil. On the other hand, the algae contain high amount of water and low amount of dry matter. The dry matter contain approximately 30 % of oil. The rest of dry matter could be used as feed for farm animal [6].

Recently, the biofuels of second and third generation are denoted as advanced biofuels.

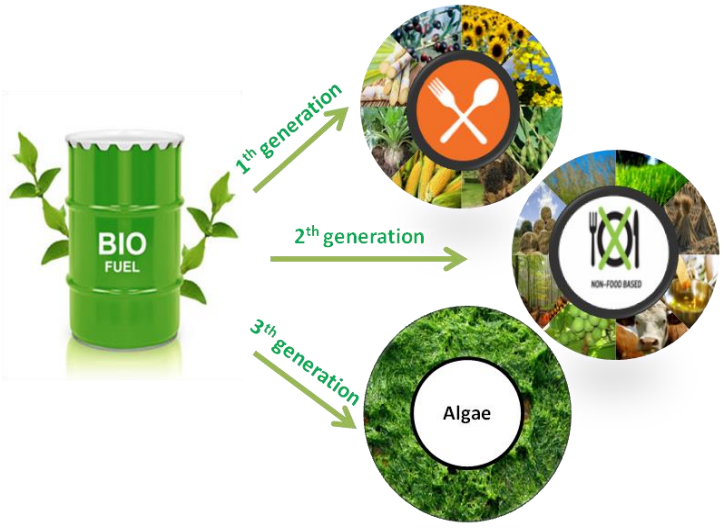

Figure 1: *Distribution of biofuels*

2.1 Biodiesel

Biodiesel is the renewable fuel, which has similar properties as diesel. It can be use without treatment of diesel engine. It has the better lubricity by the comparison with diesel. This property increased of service live of engine. Combustion of biodiesel decreased emission of CO_2 and sulfur oxides, but increased the NO_X emission. Chemically biodiesel is the mixture of esters of fatty acids and lower alcohols (methanol, ethanol and butanol). It is prepared by catalyzed reaction named transesterification (figure 1) from vegetable oils (triglycerides), animal fats or waste cooking oils. The transesterification is commonly catalyzed by homogeneous alkaline catalysts such as KOH and NaOH. The advantages of alkali catalyzed transesterification are (i) fast reaction, when during first few minutes conversion is over 90 %, (ii) lower price and (iii) easy availability of catalysts. When the sources (oil) contains higher amount of water and free fatty acids (FFA), which is typical for waste cooking oil, the soaps are formed by saponification of oil, which is caused by

alkali catalysts. Therefore, catalysts are loosed and yield of biodiesel are decreased. Two steps method is used for oil with higher amount of FFAs: the first step is esterification FFA by homogenous acid catalysts and the second steps is transesterification of triglycerides with alkali homogenous catalysts. The acid (trans-) esterification is slower than alkali transesterification, therefore is not using. The homogenous catalyst is separated from products washing of esters and so waste water is formed. This disadvantage can solve the heterogeneous catalysts, which is stable in the reaction (do not form soaps) and can be reuse after the reaction. The disadvantages of heterogeneous catalysts are the price and higher reaction condition (temperature, stirring rate, amount of methanol). The biodiesel can be prepared also without catalyst in high pressure and temperature (supercritical methanol).

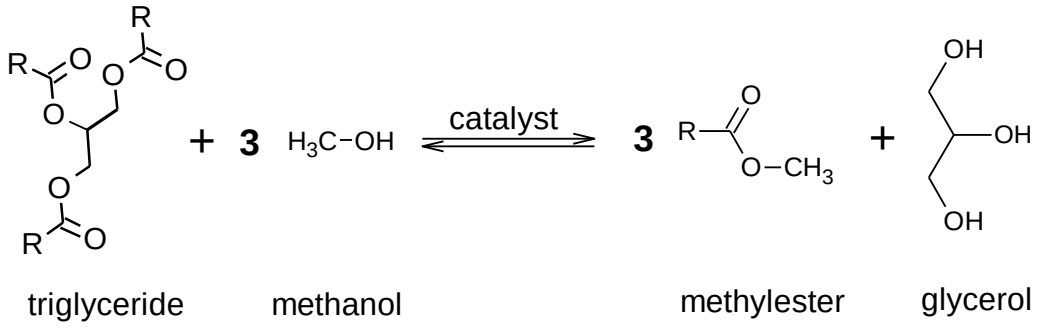

Figure 2: *Schema of transesterification*

2.2 Aldol-condensation

Under basic conditions, aldol condensation involves nucleophilic addition of an enolate ion to another carbonyl group and the product can subsequent dehydrate to form an *α, β*-unsaturated carbonyl compound. Therefore, this reaction generates C-C bonds between precursor molecules, relatively simple organic molecules as typical intermediates in biomass processing, and leads to adducts, which are platform compounds for gasoline and diesel-fuel synthesis [7]. Aldol condensation of carbonyl compounds is followed hydrogenation (C=C aliphatic, C=O ketone and C=C furanic ring bonds) and deoxygenation (via dehydration or C-OH hydrogenolysis) to yield *n*-alkanes and branched hydrocarbons with targeted molecular weight [8].

Contemporary research has been directed toward the sustainable utilization of renewable resources in an attempt to replace the dwindling fossil fuels supply.

The primary objective of these efforts is to minimize unfavourable environmental impacts and avoiding competition with food and fodder production [9]. The main attention is paid to the chemical potential of lignocellulosis biomass – especially hemicelullose, which can be transformed into C_5 and C_6 sacharide monomers via acid-catalyzed hydrolysis [8]. Sugar fractions can be further processed to furanic compounds leading to the production of hydroxymethylfurfural, furfural and other furan derivatives. These are often denoted as platform chemicals and could play the role of fundamental building blocks in future biorefineries [9].

Actually, many biomass-originated compounds have cyclic C-C rings and this structure brings up higher density by comparison with linear structure. Furfural can be obtained by acid hydrolysis of sugar cane bagasse, a residue of sugar cane processing, followed by extraction [9]. Aceton is prepared as by-products of phenol production of Cumene process. The products of aldol-condensation of furfural with acetone are 4-(2-furyl)4-hydroxybutan-2-on (FAc-OH), which is condensate to 4-(2-furyl)-3-buten-2-on (FAc). This product reacts with next furfural to 1,4-pentandien-3-on-1,5-di-2-furanyl (F_2Ac) [10, 11]. Schema of aldol-condensation acetone with furfural is on the figure 3.

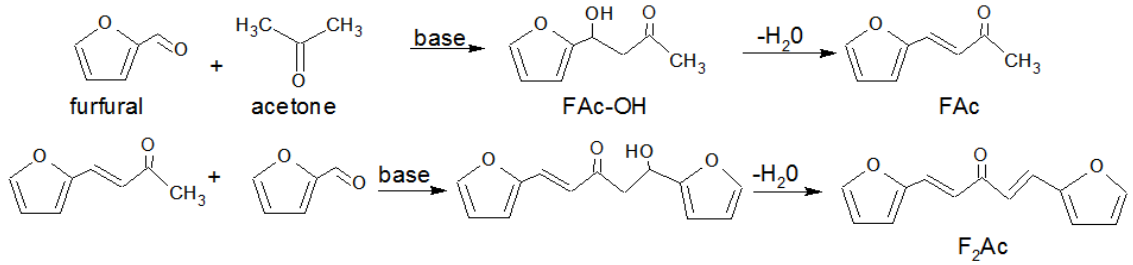

Figure 3: *Schema of aldol-condensation*

3 Hydrotalcite

Hydrotalcites (HTCs) are natural or synthetic materials belonging to layered double hydroxides (LDHs) or layered clays. The name of this group of materials “hydrotalcite” is as the some as Mg-Al hydrotalcites, which was found in Sweden around 1842 [12]. However, the first patent appeared already 1970, when the hydrotalcite was used as precursor for the preparation of catalysts of hydrogenation reactions [12].

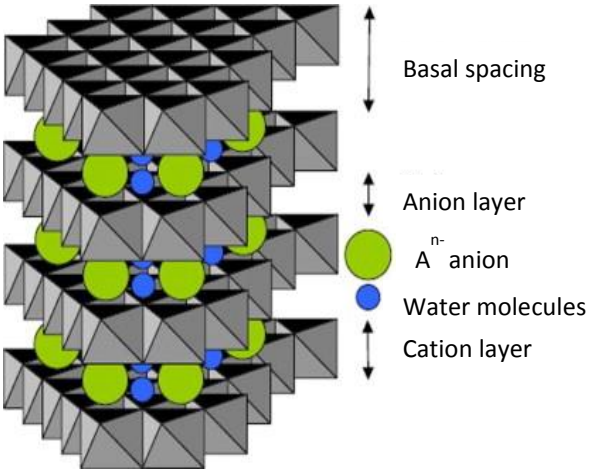

Figure 4: *Structure of hydrotalcite [13]*

Hydrotalcites have general formula $[M^{2+}_{n}M^{3+}_{m}(OH)_{2(n+m)}]^{m+}(A^{x-})_{m/x}\cdot yH_2O$, where M^{2+} and M^{3+} are divalent and trivalent metals respectively and A^{n-} is an *n*-valent anion [14]. Symbol "*x*" represented the degree of partial substitution of M^{2+} by M^{3+} and its values have been reported in the range of $0.1 \leq x \leq 0.5$, but pure phases only exist for $0.2 < x < 0.33$ [15].

Table 1: *Ionic radius of suitable cations for hydrotalcite synthesis*

M^{2+}	Be	Mg	Cu	Ni	Co	Zn	Fe	Mn	Cd	Ca
Ionic radius, Å	0.45	0.72	0.87	0.69	0.745	0.88	0.78	0.83	0.95	1
M^{3+}	Al	Ga	Ni	Co	Fe	Mn	Cr	V	Ti	In
Ionic radius, Å	0.535	0.62	0.6	0.61	0.645	0.645	0.615	0.64	0.67	0.8

Hydrotalcite has the layered structure, which is derived from brucite [$Mg(OH)_2$] by isomorphous substitution of Mg^{2+} ion, coordinating octahedrally by six OH^- anions, by a trivalent cation M^{3+} [16, 17]. The suitable cation, which could be substituted of magnesium has to have similar ion diameter as magnesium ion [12] (Table 1). From this reason, the positive charge is formed in this layer, named cation layer, which is compensated by anions which are intercalated into adjacent layers, named anion layer, in order to attain a charge neutrality [12]. The number of anions is not limited. The different types of anions can be bonded in anion layer such as various simple organic, inorganic, polyoxometalate and complex anions [12]. There are also water molecules, which are situated in the free space between the molecules of anions.

4 Result and discussion

4.1 Structure of hydrotalcites and mixed oxides

In the figure 5 are patterns of hydrotalcite with different di- and trivalent cations. On the patterns were observed the sharp and symmetric diffraction line at 2Θ ≈ 11.5, 23.2, 34.7, 39.2, 46.6, 60.6 and 62.0 ° were attributed to layered structure of hydrotalcites [18]. The diffraction lines of hydrotalcites were slightly shifted, which could be caused the by the different composition of crystal lattice. The intensive diffraction lines in the high diffraction angles was not observed on the pattern of Ca-Al hydrotalcite. The structure of Ca-Al hydrotalcite was slightly different from other hydrotalcite, because the ion diameter of Ca is high (1 Å) by comparison with magnesium (0.72 Å) and calcium is slightly shifted in the crystal lattice, which is not regular as by Mg-Al hydrotalcite. On the other hand, the new diffraction lines at 2Θ ≈33.6, 37.3, 44.0, 53.0, 56.5, 63.8 and 65.5 ° were observed by Zn-Al hydrotalcite. These diffraction lines are characteristic for ZnO [19].

.

$$D = \frac{K \cdot \lambda}{\beta \cdot cos\theta} \quad (1)$$

The prepared hydrotalcites had high crystallinity. The crystal size was calculated by Scherrer equation (1), where *D* is crystal size (nm) *K* is shape factor (0.9 was used), λ is X-Ray wavelength (0.154056 nm), β is the broadening at half the maximum diffraction line intensity (FWHM) and Θ is Bragg angle (rad) [20]. The crystal size of hydrotalcites with different two- and trivalent cations were determined from diffraction line at 2Θ ≈ 11.5 ° and they are depicted in table 2. The crystal size of prepared hydrotalcites with different composition was different in range from 10 to 63.9 nm. The crystal size of Mg-Al hydrotalcite was the lowest, which reached 10 nm. When is the aluminium substituted by iron, the crystal size of hydrotalcite approximately was twice increased. The crystal size increased with substitution of magnesium by zinc or calcium. The calcium caused the increasing the crystal size approximately four times and zinc six times by comparison with Mg-Al hydrotalcite. The composition of hydrotalcite was significantly influenced by crystal size.

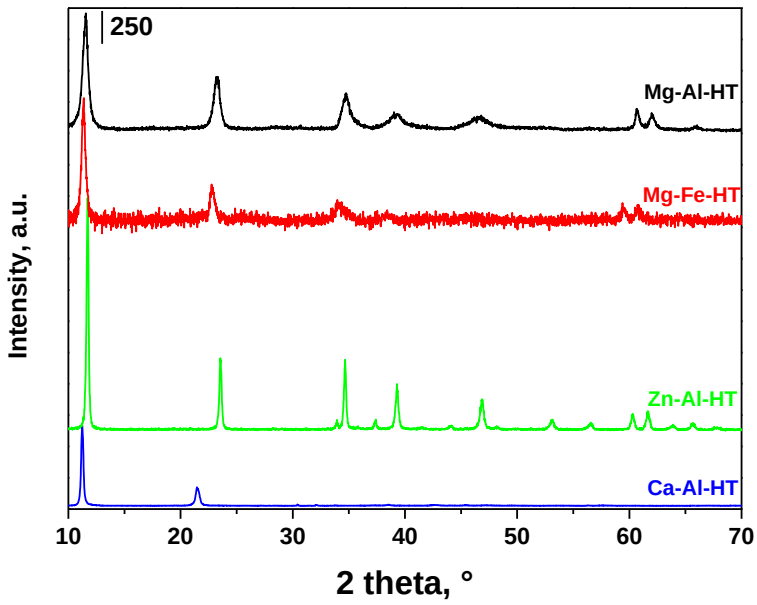

Figure 5: *Pattern of hydrotalcite with different divalent and trivalent cation*

Table 2: *Structure properties of hydrotalcites with different cations*

Hydrotalcite	*D* nm	*a* nm	*c* nm
Mg-Al-HT	10.0	0.305	2.298
Mg-Fe-HT	21.5	0.305	2.352
Zn-Al-HT	63.9	0.307	2.271
Ca-Al-HT	35.1	0.322	2.605

Hydrotalcites crystallize in rhombohedra 3R symmetry and their structure could be described by lattice parameter *a* and *c*, which are depicted in table 2. The lattice parameters were calculated from d-spacing (d_{003} and d_{110}), which correspond diffraction lines at $2\Theta \approx 11.5$ and 60.1°, respectively. The lattice parameter *a* represented of metal-metal distance in cation layer in 110 plane and the equation 2 was used for its determination. The lattice parameter *a* had the same value (0.305 nm) for Mg-Al, Mg-Fe. However, the latice parameter *a* of Zn-Al hydrotalcite was slightly higher (0.307 nm). On the other hand, the lattice parameter *a* of Ca-Al hydrotalcite was significantly higher (0.322 nm) by comparison with other type of

hydrotalcites. This difference can be caused by the higher ion diameter of calcium (1 Å) and also Zn (0.88 Å) by comparison with Mg (0.72 Å) ion.

$$a = 2 \cdot d_{110} \quad (2)$$

The lattice parameter *c* represented the distance of three cation and three anion layers. The thickness of anion layer is depended on the number, orientation strength of the bonds between anions and hydroxyls groups of cation layer [12]. The equation 3 was used for determination of the lattice parameter *c* and the values of hydrotalcites with different composition were in the range from 2.271 to 2.605 nm. The lowest value was determined at the Zn-Al hydrotalcite (2.271 nm) and slightly higher at Mg-Al hydrotalcite (2.298 nm) and at Mg-Fe hydrotalcite (2.352 nm). On the based of the values of lattice parameter *a*, it could be declined, that the value of parameter *c* depending only on the anion layer by Mg-Al, Mg-Fe and Zn-Al hydrotalcites. On the other hand, the highest value of lattice parameter *c* was determined by the Ca-Al hydrotalcite. It was with accordance with highest lattice parameter *a* of Ca-Al hydrotalcite.

$$c = 3 \cdot d_{003} \quad (3)$$

4.2 Decomposition of hydrotalcite to formed mixed oxides

The hydrotalcites were not thermally stable and the layered structure was collapses in the temperature up 300 °C. The gaseous compounds were released from the anion layer throughout collapsing layered structure and formation mixed oxides. The amount of releasing compounds and the temperature of structure decomposition could be studied by the thermogravimetry equipped by mass spectrometer. The TGA and dTGA curves of hydrotalcites with different composition are depicted on the figure 6.

The compounds were released during the thermal decomposition of layered structure of Mg-Al, Mg-Fe and Zn-Al hydrotalcites in the two main steps. On the other hand, the thermal decomposition of Ca-Al hydrotalcite was different and four main steps of weight loss were observed.

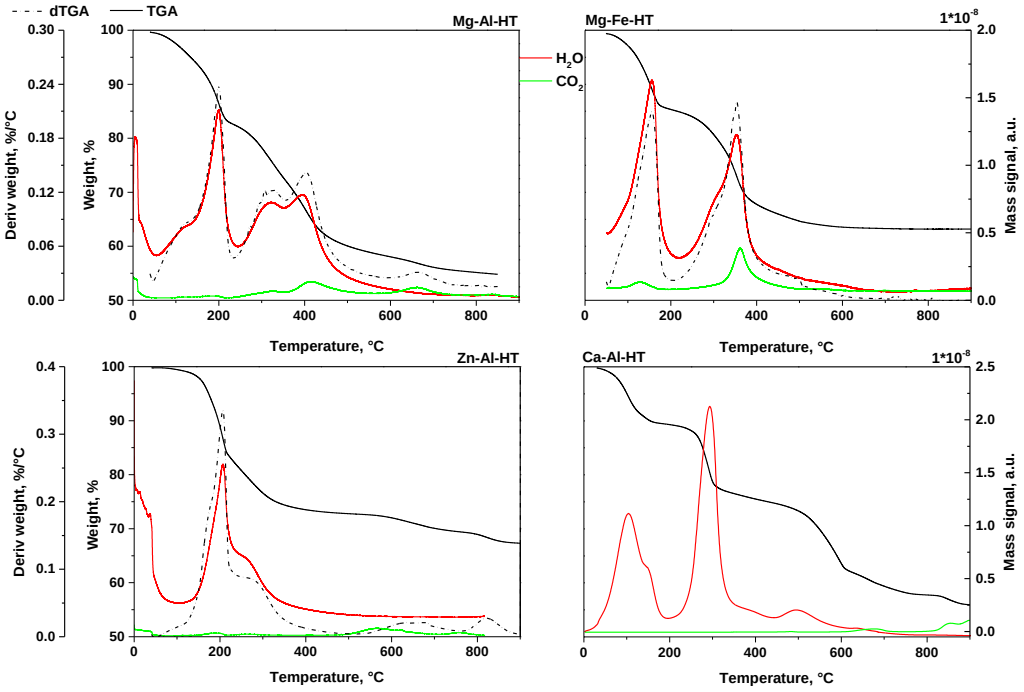

Figure 6: *TGA and dTGA curves of hydrotalcite with different composition*

The physically adsorbed water and water in anion layers was released at the first step in the temperature range from 40 to approximately 230 °C. The small amount of CO_2 was also released in the first step by Mg-Fe hydrotalcite. Two signals with maximum at 116 and 202 °C were observed on the dTGA curve of Mg-Al hydrotalcite. The temperature maximum of the first step was similar for Zn-Al and Mg-Al hydrotalcite. However, the temperature maximum decreased to 154 °C for Mg-Fe hydrotalcite. The same trend was also observed for amount of released matter which was in the range from 17.72 to 15.02 wt.%. The similar weight loss was observed for Mg-Al and Zn-Al hydrotalcite in first step, which was 17.39 and 17.72 wt.%, respectively. A little less amount of matter was released from Mg-Fe hydrotalcite (15.02 wt.%).

In the second step, which was in the temperature range approximately from 230 to 600 °C, the CO_2 and H_2O were released. In this step, the decarboxylation and dehydroxylation of anion layer were observed [21]. The dTGA curves of Mg-Al and Mg-Fe were distinguished on two signals. For Mg-Al mixed oxides were the temperature maximum at 323 and 406 °C and for Mg-Fe at slightly lower

temperature at 306 and 354 °C. The temperature maximum for Zn-Al hydrotalcite was at 283 °C. However, the major amount of CO_2 was released by Zn-Al hydrotalcite at higher temperature up 600 °C, how is observed on the figure 6. The amount of weight loss is similar for Mg-Al and Mg-Fe hydrotalcite and reached 24.70 and 21.58 wt. %, respectively. On the other hand, only 9.35 wt. % of matter was released from Zn-Al hydrotalcite in the second step.

Table 3: *TGA analyses of hydrotalcite with different composition*

Sample	1.step		2.step		3.step		4.step		Total
	T_{max} °C	w_{loss} %	T_{max} °C	w_{loss} %	T_{max} °C	w_{loss} %	T_{max} °C	w_{loss} %	w_{loss} %
Mg-Al-HT	202	17.4	404 (323)	24.7	-	-	-	-	45.3
Mg-Fe-HT	154	15.0	354 (306)	21.6	-	-	-	-	37.0
Zn-Al-HT	208	17.7	283	9.4	-	-	-	-	32.8
Ca-Al-HT	104	10.4	291	15.0	494	12.1	675	6.4	44.0

The process of thermal decomposition was different for Ca-Al hydrotalcite. In the three steps were released water in the temperature range from 40 to 181 °C, from 181 to 446 °C and from 460 to 617 °C with temperature maximums at 104, 291, 494 °C, respectively. In the first step was released 10.44 wt. %, in the second step 15.04 wt. % and 12.04 wt. % in the third step. The CO_2 released in four step, which was in temperature range from 617 to 777 °C.

The total weight loss of hydrotalcites with different composition was in the range from 32.77 to 45.30 wt.%. The lower weight loss was observed by Zn-Al hydrotalcite, only 32.77 wt.%. Slightly high weight loss was observed at the Mg-Fe hydrotalcite (37.00 wt.%). The similar weight loss was observed by Mg-Al and Ca-Al hydrotalcite and it was 45.30 and 44.04 wt.%. On the based of results from TGA, the suitable temperature of calcination was determined.

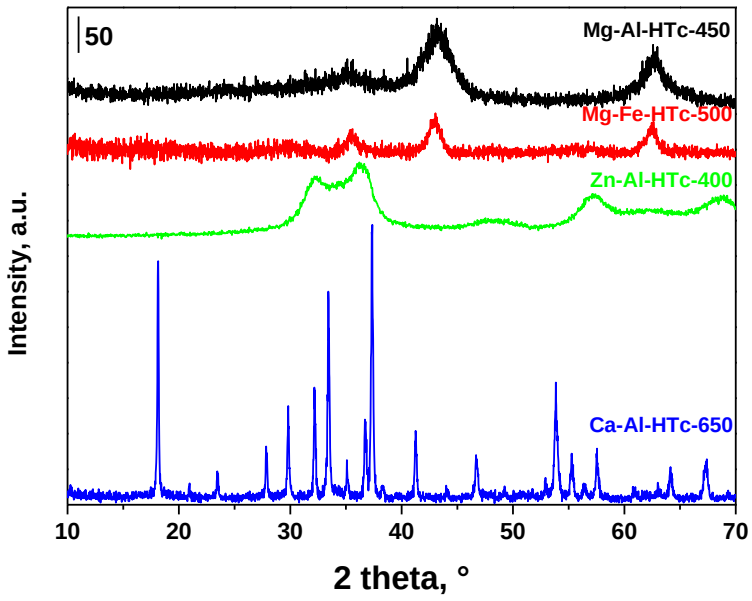

Figure 7: *XRD pattern of mixed oxides*

The mixed oxides were formed by the thermal pre-treatment of hydrotalcites at high temperatures. The layered structure was collapsed and the mixed oxides were formed. When the temperature was higher than approximately 600 °C, the spinel was formed. The structure of mixed oxides was studied by the XRD and the patterns are presented on figure 7. The diffraction lines at 2θ = 43.5 and 63.0°, which represented the MgO were observed on the XRD pattern of Mg-Al and Mg-Fe mixed oxides. On the XRD pattern of Zn-Al mixed oxides were observed of the diffraction lines at 2θ = 32.1, 34.3, 36.4 and 57.1°, which are characterized for ZnO [19]. The XRD pattern of Ca-Al mixed oxides showed the diffraction lines at v 2θ = 18.0, 29.6, 33.3, 36.6, 42.0, 46.6, 54.9 and 57.2°, which are represented the mayenite [22]. Moreover, still diffraction lines was observed at 2θ = 32.2, 37.4, 53.8, 64.0 and 67.3°, which are characteristic for cubic CaO [23]. The Ca-Al mixed oxides contained two crystal phases, CaO and mayenite. Other mixed oxides was represented only one type of crystal phase.

The diffraction lines for the Mg-Al, Mg-Fe and Zn-Al mixed oxides were not sharp. It demonstrated of the lower crystallinity. MgO, ZnO, Al_2O_3 and Fe_2O_3 were not separated phases, but that MgO was homogenously dispersed on the Al_2O_3 and

Fe_2O_3 and ZnO on Al_2O_3. On the other hand, the diffraction lines for CaO and mayenite were sharp, which shows on the high crystallinity of the sample.

Table 4: *Structure properties of mixed oxides*

Mixed oxides	2 theta, °	*D*, nm	S_{BET}, m^2/g
Mg-Al-HTc-450	43.5	2.4	113
Mg-Fe-HTc-500	43.5	6.2	85
Zn-Al-HTc-400	31.7	3.7	155
Ca-Al-HTc-650	32.4	50	-

In table 4 are presented the crystal sizes of mixed oxides. The crystal size was lower by comparison with Mg-Fe, Mg-Al and Zn-Al hydrotalcite and it was in the range from 2.4 to 6.2 nm. The lowest crystal size was observed by the Mg-Al mixed oxide. The crystal size of Zn-Al mixed oxide decreased from 63.9 nm (for Zn-Al hydrotalcite) to 3.7 nm in the course of calcination. The Mg-Fe mixed oxide had approximately three times larger crystal size by comparison with Mg-Al mixed oxides. The decreasing of crystal size during transformation the hydrotalcite to mixed oxides by thermal pre-treatment was caused by the collapsing of layered structure, which was crystalline and formation the mixed oxides with low crystallinity. However, the crystal size by Ca-Al mixed oxide was higher than by Ca-Al hydrotalcite. The mayenite, for which was the crystal size calculated, was highly crystalline material with crystal size of 50 nm.

The surface area of the hydrotalcites were lower by comparison with the mixed oxides. It was caused by the higher crystal size of hydrotalcites. The specific surface area was measured by N_2-physisorption at the temperature of liquid nitrogen (77 K). From adsorption isotherm could be determined the specific surface area of studied sample, the shape of pores and their distribution.

The specific surface area was determined by adsorption isotherm for used of BET method (S_{BET}). S_{BET} of hydrotalcites were in the range from 30 to 79.6 m^2/g. Mg-Al and Zn-Al surface area was similar and reached values of 30 and 39 m^2/g respectively. However the crystal size of Mg-Al and Zn-Al was different and reached values 10 and 63.9 nm respectively. Mixed oxides, which were formed by calcination had higher specific surface area (from 85 to 155 m^2/g).

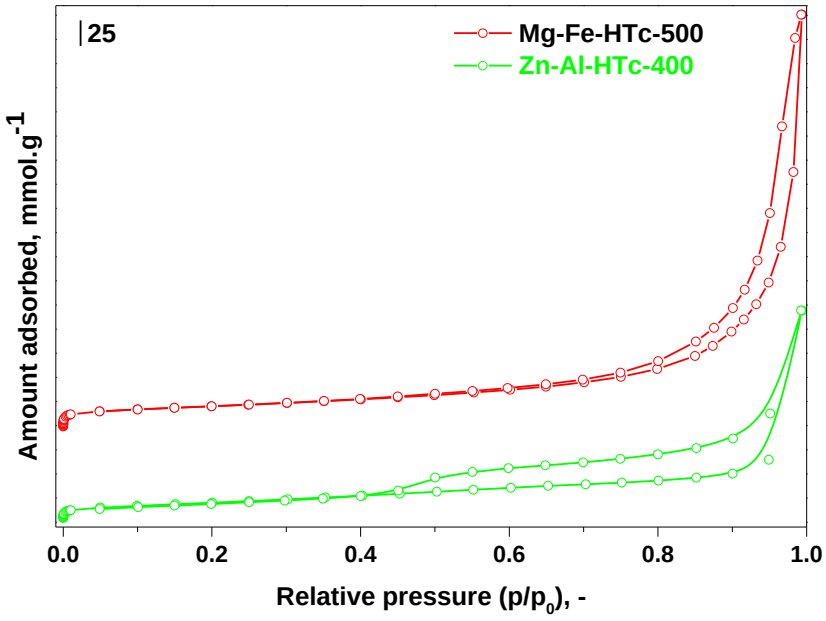

Figure 8: *N_2 adsorption isotherms of Mg-Fe and Zn-Al mixed oxide*

On the figure 8 are depicted the adsorption-desorption isotherms of Mg-Fe and Zn-Al mixed oxides. The adsorption-desorption isotherms with the hysteresis loops are characteristic for the mixed oxides prepared from hydrotalcites. Isotherms are classified as the IV type of isotherms (IUPAC) and identify mesoporous materials. Said type of hysteresis loop shows on the plate-like materials with slit-shaped pores, which have the non-rigid aggregates.

4.3 Acid-basic properties of mixed oxides

The study of acid-basic properties is the key part of the heterogeneously acid-basic catalysts study. The acid-basic properties was studied by temperature programmed technique (TPD-CO_2 and TPD-NH_3), spectroscopic technique with adsorption of probe molecules (FTIR-CO_2) and adsorption microcalorimetry. Every technique provides slightly different information about the strength, distribution and amount the acid-basic sites and collection the results from different techniques provides the deep information about acid-basic properties of studied materials.

The hydroxide anions are bonded on catios in anion layer. Besides the hydroxide anion, carbonated were situated in anion layer. However, the hydroxide anions are the Brönsted basic sites. The thermal decomposition of hydrotalcite structure and

formation of mixed oxide caused the transformation of Brönsted to Lewis basic sites. The Lewis basic sites could be transformed back on Brönsted basic sites by rehydration. The amount of basic sites, amount of hydroxide anion increased after rehydration by comparison with originated hydrotalcite. Therefore the process rehydration of mixed oxides are used commonly for preparation of rehydrated mixed oxides, which are more active in aldol-condensation reactions [24]. The mixed oxides have three types of active basic sites, which were also confirmed by CO_2 adsorption with FTIR detection [25]. The weak basic sites are represented the OH^- species and they react with CO_2 and formed the bicarbonate complexes on the surface of mixed oxides, which are observed on FTIR spectra in the region from 1150 to 1350 cm^{-1} [26]. The medium basic sites are represented the Mg^{2+} - O^{2-} and Al^{3+} - O^{2-} pairs. On the FTIR the medium basic sites are observed after adsorption of CO_2 as bidentate carbonates (chelating and bridges) in regions 1650-1800 cm^{-1} [26]. The unidentate carbonates are stable carbonate complexes, which are observed in the region 1350-1600 cm^{-1}. Unidentate carbonates are formed after adsorption of CO_2 on the strong basic sites, which are O^{2-} [26].

The standard method for determination of total amount of basic and acidic sits is temperature programmed desorption with probe molecules. The probe molecules of CO_2 was used for the determination of total number of basic sites.

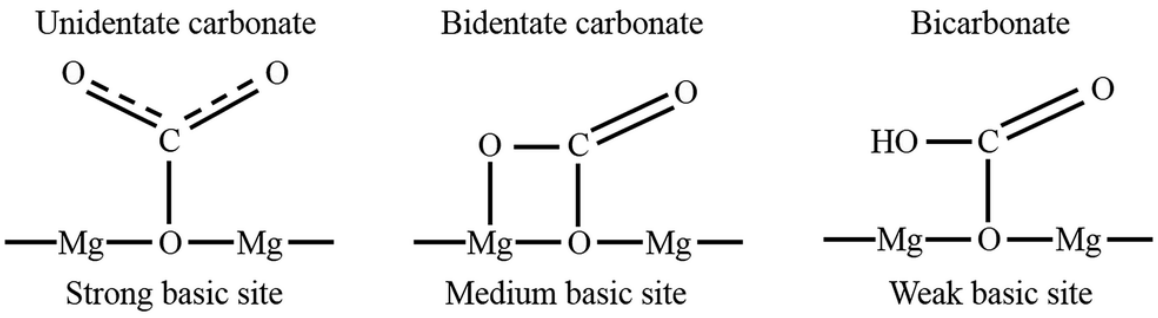

Figure 9: *The carbonate complexes bonded on the basic sites* [27]

On the figure 10 are depicted TPD-CO_2 curves of Mg-Al, Mg-Fe and Zn-Al mixed oxides. The total amount of basic sites, which corresponds with area under curves, decreased from Mg-Al > Mg-Fe > Zn-Al. The TPD curves were broad in range temperature from 35 to approximately 450 °C, which shows on high heterogeneity of mixed oxides surface. The intensive temperature maximum of curves was

observed at 91 °C for Mg-Al mixed oxides. The temperature maximum was shifted to high temperature, Mg-Fe mixed oxide had the temperature at 96 °C and Zn-Al mixed oxides even at 131 °C. The three types of basic sites could not be distinguished from these TPD curves. At first, the CO_2 were released from weak basic sites, which was approximately 120 °C for Mg-Al mixed oxides [28]. The medium basic sites could be observed on the TPD-CO_2 curve with temperature maximum at approximately 170 °C [28]. In the last step, the CO_2 from strong basic sites were released at high temperature, because is strong bonded. The strong basic sites were represented by Mg-Al mixed oxides the temperature maximum at approximately 270 °C [147].

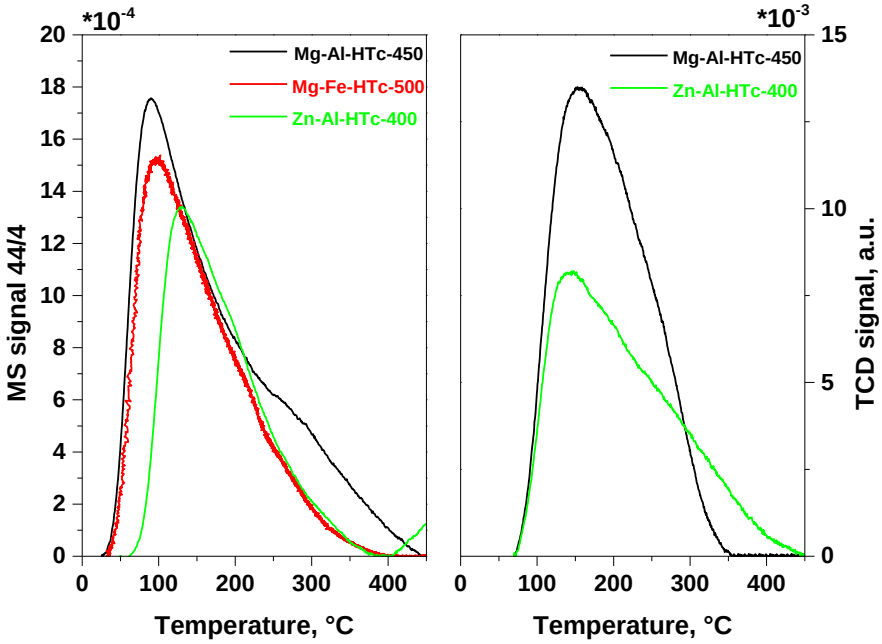

Figure 10: *TPD-CO_2 and TPD-NH_3 curves*

One of the methods for determination total amount of basic sites is TPD-NH_3. The adsorption was carried out at 70 °C for avoid to physical adsorption of ammonia, which could increased the total amount of desorbed NH_3 and amount of acid sites [29]. The ammonia is chemically adsorbed by chemical bond between nitrogen and Lewis acid sites, which are represented by unsaturated metal cation. Simultaneously, the nitrogen is linked to the nearest basic oxygen or hydroxide group by hydrogen bond. Part of ammonia could be heterolytically dissociated on NH_2^-, which carried out on acid-basic pairs partially includes basic oxygen [29].

On the figure 10 the TPD-NH_3 curves of Mg-Al and Zn-Al are depicted. The total amount of acid sites were determined from area under TPD-NH_3 curve. Mg-Al mixed oxide contained the high amount of total acid sites by comparison with Zn-Al mixed oxides. The TPD curves were broad in range temperature from 70 to approximately 450 °C, which showed on high heterogeneity of mixed oxides surface. The curve had intensive temperature maximum at 144 °C for Zn-Al mixed oxide. The temperature maximum was shifted to high temperature in Mg-Al mixed oxide, which was at 153 °C.

4.4 Catalytic results in aldol-condensation and transesterification

The prepared mixed oxides were studied in aldol-condensation of furfural with acetone and transesterification of rapeseed oil with methanol. Both reactions are used for biofuel production.

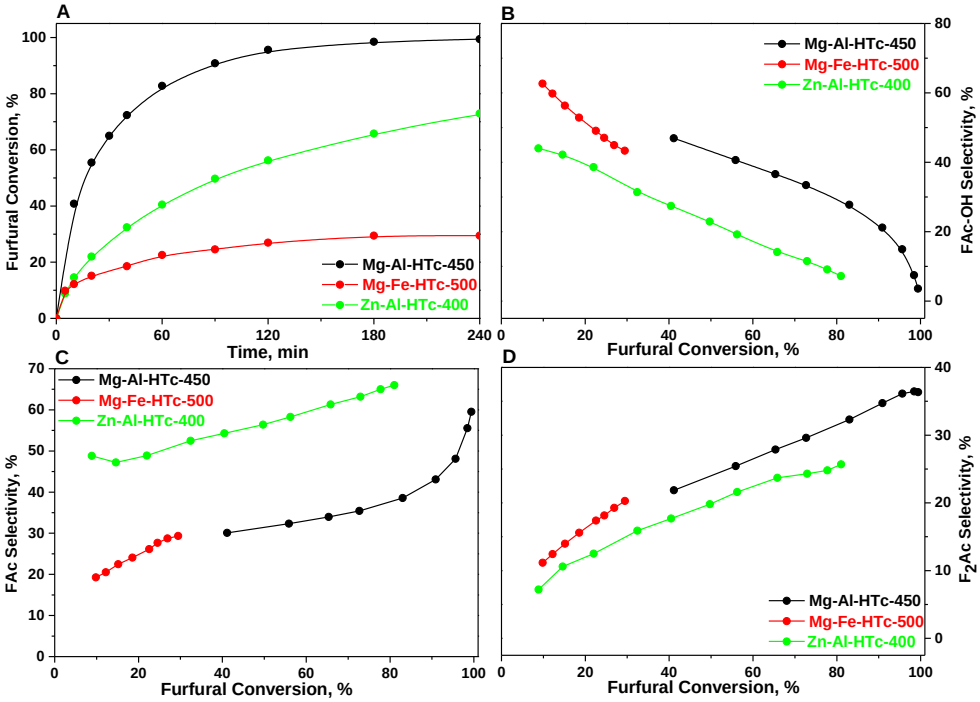

Figure 11: *Catalytic results of Mg-Al, Mg-Fe and Zn-Al mixed oxides in aldol condensation*

Mg-Al, Mg-Fe and Zn-Al mixed oxides was tested in aldol-condensation furfural with acetone and the catalytic results are in the figure 11. The aldol-condensation was studied at these reaction condition: temperature 50 °C, stirring rate 320 rpm, 4.6 wt. % of catalyst to reaction mixture, 10:1 molar ratio acetone:furfural, 6.5 g

furfural. The reaction rate increased in this order Mg-Fe-Htc-500 < Zn-Al-HTc-400 < Mg-Al-HTc-450. The furfural conversion reached 30, 72 and 88 % by Mg-Fe, Zn-Al and Mg-Al after 4 hours respectively.

The selectivity of main products was also determined (Fig) 11. The selectivity of FAc-OH decreased with increasing the conversion of furfural. On the other hand the selectivity of two main condensate products (FAc and F2Ac) increased with increasing of the furfural conversion. The selectivity of the FAc (at the same furfural conversion) is higher for used of Zn-Al mixed oxide than Mg-Al mixed oxide. Controversially, The F2Ac selectivity (at the same furfural conversion) was slightly higher for used Mg-Al mixed oxide than Zn-Al mixed oxide. In the low furfural conversion of Zn-Al mixed oxides can be compared the selectivity to main products for Zn-Al and Mg-Fe mixed oxides. The selectivity of FAc was higher for Zn-Al than for Mg-Fe mixed oxide. However, the selectivity of F2Ac was higher for Mg-Fe than for Zn-Al mixed oxides. The selectivity confirmed, that the furfural with acetone reacted according to designed reaction schema on figure 11.

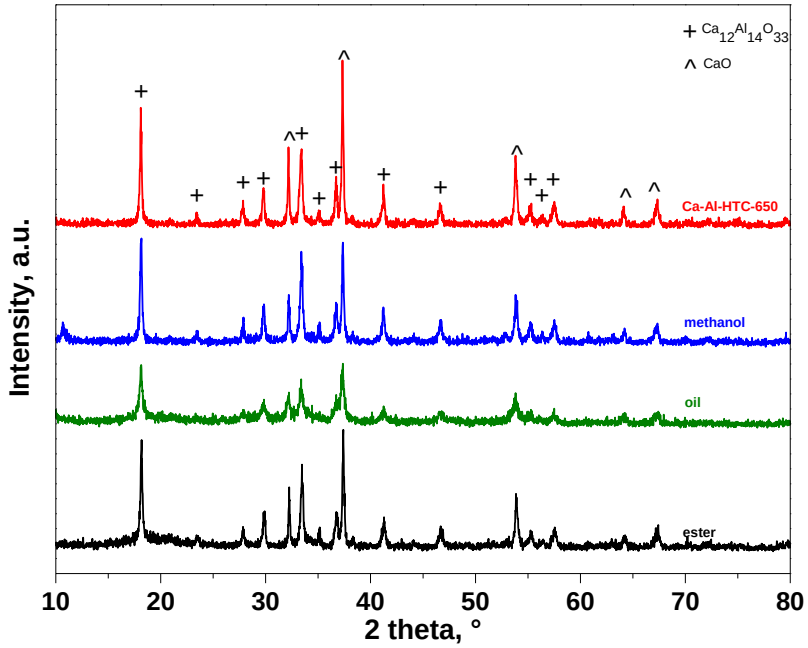

Figure 12: *Stability of Ca-Al mixed oxides in the main compounds of reaction*

Texture, structure and acid-basic properties of catalysts are necessary to know for the explanation of the catalytic data in detailed. The furfural conversion increased with decreasing of the crystal size. The specific surface area of mixed oxides was

slightly higher for Zn-Al than for Mg-Al, however, the conversion was higher for Mg-Al than Zn-Al mixed oxides. The lowest surface area was determined for Mg-Fe mixed oxide, which was in the correlation with furfural conversion. Mixed oxides were mesoporous materials, which was confirmed by N_2-izotherms. The highest amount of the basic sites was observed by the Mg-Al mixed oxides, which is in the correlation with furfural conversion. The total amount of basic sites was slightly higher for Mg-Fe mixed oxide than Zn-Al mixed oxide. However, the furfural conversion was lower for Mg-Fe than Zn-Al mixed oxide.

Controversially, the Ca-Al mixed oxide was tested in transesterification of rapeseed oil with methanol. The conditions of transesterification were following: reaction temperature 65 °C, methanol:oil molar ratio 24:1, 3.4 wt.% of catalyst to oil, stirring rate 320 rpm, 25 g of rapeseed oil. The yield of methylesters was 99 % for Ca-Al mixed oxide after 8 hours. The stability of Ca-Al mixed oxide was also tested. It was found, that the mixed oxide (mayenit and CaO) was stable in oil, methanol and methylesters, but not in the glycerol. The stability was also confirmed by XRD, where the diffraction lines for CaO and mayenit was observed after stability test (catalyst was mixing with the one of the reaction compounds). The stability test showed, that during the reaction the CaO is leached from the catalyst and the mayenite was stable phase in the catalysts.

5 Conclusion

The thesis was focused on the study of Mg-Al, Mg-Fe, Zn-Al and Ca-Al mixed oxides, which were tested as catalysts in the aldol-condensation of furfural with acetone and the transesterification rapeseed oil with methanol. The theses describe the (i) structure, (ii) texture and acid-basic properties of mixed oxides with different compositions and explained the catalytic properties.

The hydrotalcite with the different contain of metals was successfully synthesized by co-precipitation method. The different properties of hydrotalcites and mixed oxides with the same molar ratio $M^{2+}/M^{3+} = 2$ were observed. The lattice parameter *a* showed that the Ca-Al has slightly different structure, which was caused by the large size of calcium (1 Å) in comparison with magnesium (0.72 Å). Therefore the

calcium is slightly shifted in the crystal lattice by the comparison with other hydrotalcites.

Mg-Al, Mg-Fe and Zn-Al mixed oxides were tested in aldol-condensation of furfural with acetone. The conversion of furfural reached 99, 71 and 30 % for Mg-Al, Zn-Al and Mg-Fe mixed oxides respectively. However, the selectivity of main products was different. Zn-Al mixed oxide was more selective to FAc and the Mg-Al and Mg-Fe more selective to F2Ac. It can be explained by the different distribution of basic sites. The Mg-X mixed oxides has the higher population of strong basic sites, which are participating on the dehydratation of FAc to F2Ac. On the other hand, the acid cites are participating on the dehydratation of FAc-OH to FAc. Contrariwise, Zn-Al mixed oxides contained small population of strong basic sites, therefore the selectivity of FAc was higher in comparison with Mg-X mixed oxides. The higher furfural conversion of Zn-Al mixed oxides in comparison with Mg-Fe could be explained by specific surface area and crystal size. For Zn-Al mixed oxide was determined the specific surface area 155 m^2/g and crystal size 3.7 nm against Mg-Fe mixed oxide with specific surface area only 85 m^2/g and crystal size 6.2 nm. The adsorption-desorption isotherms confirmed, that the mixed oxides are mesoporous materials.

The Ca-Al mixed oxide was tested in transesterification of rapeseed oil with methanol. The yield of methylesters reached 99 % after 8 hours. However the calcium was determined in the reaction mixture. The Ca-Al mixed oxide (catalyst) contained mayenite and CaO. It was found, that the mayenite was stable in the transesterification, but CaO leached from the catalyst. Therefore the stability of the Ca-Al mixed oxide was tested in rapeseed oil, methanol, methylesters and glycerol and it was found that the catalyst is not stable in glycerol.

6 References

1. Hoekman, S.K., *Biofuels in the US - Challenges and Opportunities.* Renewable Energy, 2009. **34**(1): p. 14-22.
2. Sims, R.E.H., et al., *An overview of second generation biofuel technologies.* Bioresource Technology, 2010. **101**(6): p. 1570-1580.
3. van Eijck, J., B. Batidzirai, and A. Faaij, *Current and future economic performance of first and second generation biofuels in developing countries.* Applied Energy, 2014. **135**: p. 115-141.
4. Alaswad, A., et al., *Technologies and developments of third generation biofuel production.* Renewable & Sustainable Energy Reviews, 2015. **51**: p. 1446-1460.
5. Mohr, A. and S. Raman, *Lessons from first generation biofuels and implications for the sustainability appraisal of second generation biofuels.* Energy Policy, 2013. **63**: p. 114-122.
6. Smith, A.L., et al., *Second generation biofuels and bioinvasions: An evaluation of invasive risks and policy responses in the United States and Canada.* Renewable & Sustainable Energy Reviews, 2013. **27**: p. 30-42.
7. Hora, L., et al., *Comparative study of physico-chemical properties of laboratory and industrially prepared layered double hydroxides and their behavior in aldol condensation of furfural and acetone.* Catalysis Today, 2015. **241**: p. 221-230.
8. Ramos, R., et al., *Solvent effects in hydrodeoxygenation of furfural-acetone aldol condensation products over Pt/TiO2 catalyst.* Applied Catalysis a-General, 2017. **530**: p. 174-183.
9. Hora, L., et al., *Aldol condensation of furfural and acetone over Mg-Al layered double hydroxides and mixed oxides.* Catalysis Today, 2014. **223**: p. 138-147.
10. Xing, R., et al., *Production of jet and diesel fuel range alkanes from waste hemicellulose-derived aqueous solutions.* Green Chemistry, 2010. **12**(11): p. 1933-1946.
11. Kikhtyanin, O., et al., *Peculiar behavior of MWW materials in aldol condensation of furfural and acetone.* Dalton Transactions, 2014. **43**(27): p. 10628-10641.
12. Cavani, F., F. Trifiro, and A. Vaccari, *Hydrotalcite-Type Anionic Clays: Preparation, Properties and Applications.* Catalysis Today, 1991. **11**(2): p. 173-301.
13. Duan, P., et al., *Influence of layered double hydroxides on microstructure and carbonation resistance of sulphoaluminate cement concrete.* Construction and Building Materials, 2013. **48**: p. 601-609.
14. Yang, G., J.Q. Jiang, and Y.W. Zhang, *Synthesis of cyclohexanone-formaldehyde resin catalyzed by rehydrated Mg-Al hydrotalcite.* Progress in Organic Coatings, 2015. **78**: p. 55-58.
15. Delidovich, I. and R. Palkovits, *Structure-performance correlations of Mg-Al hydrotalcite catalysts for the isomerization of glucose into fructose.* Journal of Catalysis, 2015. **327**: p. 1-9.
16. Ghorbel, S.B., et al., *Phosphoric acid intercalated Mg-Al hydrotalcite-like compounds for catalytic carboxylation reaction of methanol in a continuous system.* Applied Catalysis a-General, 2015. **493**: p. 142-148.

17. Nawfal, M., et al., *Hydrogen production by methane steam reforming over Ru supported on Ni-Mg-Al mixed oxides prepared via hydrotalcite route.* International Journal of Hydrogen Energy, 2015. **40**(2): p. 1269-1277.
18. Cantrell, D.G., et al., *Structure-reactivity correlations in MgAl hydrotalcite catalysts for biodiesel synthesis.* Applied Catalysis a-General, 2005. **287**(2): p. 183-190.
19. Jiang, W., et al., *Preparation, application, and optimization of Zn/Al complex oxides for biodiesel production under sub-critical conditions.* Biotechnology Advances, 2010. **28**(5): p. 620-627.
20. Parra, M.R. and F.Z. Haque, *Aqueous chemical route synthesis and the effect of calcination temperature on the structural and optical properties of ZnO nanoparticles.* Journal of Materials Research and Technology-Jmr&T, 2014. **3**(4): p. 363-369.
21. Morato, A., et al., *Palladium hydrotalcites as precursors for the catalytic hydroconversion of CCl2F2 (CFC-12) and CHClF2 (HCFC-22).* Applied Catalysis B-Environmental, 2001. **32**(3): p. 167-179.
22. Kocik, J., M. Hajek, and I. Troppova, *The factors influencing stability of Ca-Al mixed oxides as a possible catalyst for biodiesel production.* Fuel Processing Technology, 2015. **134**: p. 297-302.
23. Lee, H.V., et al., *Heterogeneous base catalysts for edible palm and non-edible Jatropha-based biodiesel production.* Chemistry Central Journal, 2014. **8**.
24. Kikhtyanin, O., et al., *Reconstructed Mg-Al hydrotalcites prepared by using different rehydration and drying time: Physico-chemical properties and catalytic performance in aldol condensation.* Applied Catalysis a-General, 2017. **536**: p. 85-96.
25. Hajek, M., et al., *Transesterification of rapeseed oil by Mg-Al mixed oxides with various Mg/Al molar ratio.* Chemical Engineering Journal, 2015. **263**: p. 160-167.
26. Smolakova, L., et al., *Surface Properties of Hydrotalcite-Based Zn(Mg)Al Oxides and Their Catalytic Activity in Aldol Condensation of Furfural with Acetone.* Industrial & Engineering Chemistry Research, 2017. **56**(16): p. 4638-4648.
27. Song, G., et al., *Influence of the precursor on the porous structure and CO2 adsorption characteristics of MgO.* Rsc Advances, 2016. **6**(23): p. 19069-19077.
28. Di Cosimo, J.I., et al., *Structure and surface and catalytic properties of Mg-Al basic oxides.* Journal of Catalysis, 1998. **178**(2): p. 499-510.
29. Prinetto, F., et al., *Investigation of acid-base properties of catalysts obtained from layered double hydroxides.* Journal of Physical Chemistry B, 2000. **104**(47): p. 11117-11126.